Analytical Solution of Aluminum Alloy Plates With Holes Subjected to Cold Expansion With Reverse Yielding

Abdel-Hakim Bouzid[1]
ASME Fellow
Professor
Ecole de Technologie Superieure,
1100 Notre-Dame Ouest,
Montreal, QC H3C 1K3, Canada
e-mail: hakim.bouzid@etsmtl.ca

Hacène Touahri
Ecole de Technologie Superieure,
1100 Notre-Dame Ouest,
Montreal, QC H3C 1K3, Canada
e-mail: touahri98@hotmail.com

Khaled Benfriha
Professor
AMIT, Arts et Métiers Institute of Technology,
HESAM Université, 151 boulevard de l'hôpital,
Paris 75013, France
e-mail: khaled.benfriha@ensam.eu

The expansion induced by cold working is a common process that generates residual stresses. It is used when fatigue damage accumulation and life reduction of aluminum alloy perforated plates is an issue in the aeronautics industry. This process is an attractive solution to extend the fatigue lifetime of these structures. It aims at generating residual stresses and increases thereby the strength of hollow parts including aluminum alloy plates with holes commonly used in the manufacture of airplane fuselage. Unfortunately, the life predictions require a good prediction of the residual stresses and in particular when reverse yielding takes place. An analytical model to predict the residual stresses induced during the expansion process due to the cold strain hardening is developed. The proposed analytical model is based on an elasto-plastic behavior, with a power law material behavior and relies on the theory of autofrettaged thick wall cylinders in plane strain state to which reverse yielding is incorporated. The application of Hencky theory of plastic deformation is used in the analytical calculations of the stresses and strains. Finite element numerical simulation is used to validate the developed analytical model by comparison of the radial, hoop, longitudinal, and equivalent stresses for both the loading and unloading phases. The obtained results show clearly that the level of residual stresses depend mainly on the interference and strain hardening while reverse yielding reduces the stresses near the hole. [DOI: 10.1115/1.4049490]

Keywords: cold expansion, strain hardening, residual stresses, interference, elasto-plastic behavior

Introduction

Riveted assemblies allow great flexibility in a variety of applications and are widely used in various industries, including chemical, nuclear, space, and heavy industries and more specifically in the aeronautical industry [1]. Indeed, airplane fuselage panel assemblies rely heavily on a set of riveted aluminum-alloy plates. Drilling holes through aluminum plates is a necessary step to produce riveted assemblies to form the complete structure. However, several previous studies have clearly demonstrated that these aluminum alloy plates are deformed plastically due to stress concentration around the holes during the riveting procedure [2–4]. In addition, during the flight of an aircraft, the cyclic loads induced by vibration coupled to those produced during pressurization of the cabin can cause the propagation of initiated cracks around these holes and thus produce fatigue failure of the structure [5,6]. This, in turn, limits the operability of the planes and generates a huge loss of aeronautical industry incomes due to increased maintenance and repair frequency and time. According to the available statistics, fractures and fatigue failures of fastener holes and drilled plates account for over 50% of grounded planes [6,7]. To overcome fractures and increase the fatigue life, several techniques are used: shot peening, laser shock, cold expansion, and interference fitting are to name a few. Each technique has its merits and is used in specific applications. However, without elaboration of the specifics of each technic, to avoid stress concentration and fatigue crack propagation around assembly holes, creating residual stresses around them is an attractive procedure [8,9]. Therefore, the preferred method to generate residual stresses is the one that involves expanding the hole of the plate by forcing a hard mandrel slightly bigger, and then gradually removing it. The higher residual stresses of compression type generated at the inner wall just like in autofrettaged thick-wall cylinders increase the strength of the plate considerably. This process known as cold expansion [10,11] extend the fatigue life of these joints. It reduces crack initiation and propagation, prevents premature fatigue failure and hence improves their durability. The level of residual stresses around a hole in an aluminum alloy plate depends on the oversized mandrel dimension to be drawn through it. The interference and strain hardening control the level of residual stresses obtained after the cold expansion process. In Ref. [12], Clark developed a model to predict residual stresses and crack growth in residual stress fields. The model is based on an elastic perfectly plastic material behavior with a modified Tresca yield criterion to avoid complexity in providing the critical crack length.

The expansion process due to cold strain hardening has received special attention from scientists and technologists since a long time. Several analytical and numerical models were developed to predict residual stresses [13,14]. A model was developed by Hsu and Forman [15], whose analysis focused on the stresses and strains at the inner wall of a hole subjected to internal pressure in the case of an infinite plate. The analysis was made under the plane stress condition and uses the von Mises yield criterion. However, this model does not take into account the fact that during unloading or the retrieve of the mandrel, a small zone at the bore may develop reverse plastic yielding but considers the plate to be subjected to a purely elastic recovery instead. Using Budiansky's theory and a modified Ramberg-Osgood law, Guo [16] developed an exact elastic–plastic solution of a finite circular sheet having a cold-worked hole. The residual stresses obtained agree with the numerical FE and experimental results. Based on

[1]Corresponding author.

Contributed by the Pressure Vessel and Piping Division of ASME for publication in the Journal of Pressure Vessel Technology. Manuscript received March 24, 2020; final manuscript received November 24, 2020; published online February 11, 2021. Assoc. Editor: Reza Adibi-Asl.

J2 deformation theory and taking into account Bauschinger effect, the model by Wang [17] was compared to the models by Nadai [13] and Hsu [15] that do not include reverse plasticity.

Poussard et al. [18] conducted a two-dimensional finite element study to simulate the 4% cold working of a 6.35 mm diameter hole in a 6 mm thick aluminum alloy plate. The finite element results were compared to earlier analytical models and found major differences due to reverse yielding. In contrast to this study, Ball [19] enlarged the domain by including the phenomenon of the reverse plasticity during the unloading process. In addition, this study included Bauschinger effect. Then, to validate the model, he used experimental measurements obtained by the X-ray diffraction method. Furthermore, many other studies have been carried some of which considered the interaction between the mandrel and the plate. Lapalme [20] presented a three-dimensional aspect of the process through a physical illustration of the problem, the aim of which was to develop a numerical simulation method introducing different elements involved in the cold expansion process, in order to consider their impact on the hardened hole. To do this, a finite element method (FEM) was developed to characterize the residual stresses of the process. Then, the simulation model was validated by experimental measurements obtained from nondestructive methods, including X-ray diffraction, digital image correlation, and optical measurements.

This study focuses on the residual stresses of the different zones near the bore of the aluminum alloy plate shown in Fig. 1. The analytical model development that leads to the prediction of the residual stresses is rather complex but is worth the effort since it can be used as a supplement tool to FEM or testing [21–23] while giving relatively much faster answers. The analytical model is developed for plates made of aluminum alloys with a power law material behavior law [24,25] subjected cold expansion process. The model is based on the theory of autofrettaged thick-wall cylinders in plane strain state and integrates the effect of reverse yielding that alleviates the stresses at the bore. Finally, the analytical model is confronted to the finite element numerical modelling by comparing the results of the radial, hoop, longitudinal, and equivalent stresses generated in an aluminum alloy plate.

Analytical Model

Although several cases of studies are possible, we will be interested in the particular case of the expansion of the plate without plastic deformation of the mandrel since it is made with a higher strength material. In the analysis, the aluminum alloy plate (Al-7050-T73511) is considered as a hollow cylinder with a finite outer diameter, and the mandrel in steel (AISI 4340) is considered as a solid shaft deformable elastically.

Indeed, in practice, the mandrel must be reused several times and hence it is designed to not deform plasticity. Therefore, the analytical model of the cold expansion process is based on the following assumptions:

- The materials for both the mandrel and plate are considered to be isotropic and homogeneous. The expansion occurs without plastic deformation of the mandrel.
- The plate is considered to be under plain strain and deforms elasto-plastically and according to Ludwik power law strain hardening behavior [26].
- Reverse yielding of the plate is accounted for considering Bauschinger effect together with a different hardening exponent, elastic modulus, and Poisson's ratio that characterize the unloading behavior of some materials.

The mandrel and plate are described through the following laws of the stress–strain behaviors. For steel mandrel, the loading and unloading follow an elastic behavior

$$\sigma_e = E_m \varepsilon_e, \ \forall \sigma \tag{1}$$

For the aluminum alloy plate, the loading is an elasto-plastic behavior (applicable during expansion or when the mandrel is introduced)

$$\begin{cases} \sigma_e = E_p \varepsilon_e, & \sigma \le S_{yp} \quad \text{(section 1)} \\ \sigma_e = A + B\varepsilon_e^n, & \sigma > S_{yp} \quad \text{(section 2)} \end{cases} \tag{2}$$

For the unloading, the behavior is similar with relatively higher yield as shown in Fig. 2, (applicable after removing the mandrel from the hole)

$$\begin{cases} \sigma_e = E_{pu} \varepsilon_e, & \sigma \le S_{\text{ypu}} \quad \text{(section 3)} \\ \sigma_e = A_u + B_u \varepsilon_e^{n_u}, & \sigma > S_{\text{ypu}} \quad \text{(section 4)} \end{cases} \tag{3}$$

Figure 3 shows the three deformed zones near the hole of the aluminum plate; the elastic zone, the plastic zone, and the reverse yielding zone. In the cylindrical coordinates system (r, θ, and z) and in the case of elasto-plastic behavior, the expressions of the equivalent stress σ_e and equivalent strain ε_e, respectively, defined by the second invariant of the tensors stresses and strain, are given by

$$\sigma_e = \sqrt{\frac{1}{2}\left[(\sigma_r - \sigma_\theta)^2 + (\sigma_\theta - \sigma_z)^2 + (\sigma_z - \sigma_r)^2\right]} \tag{4}$$

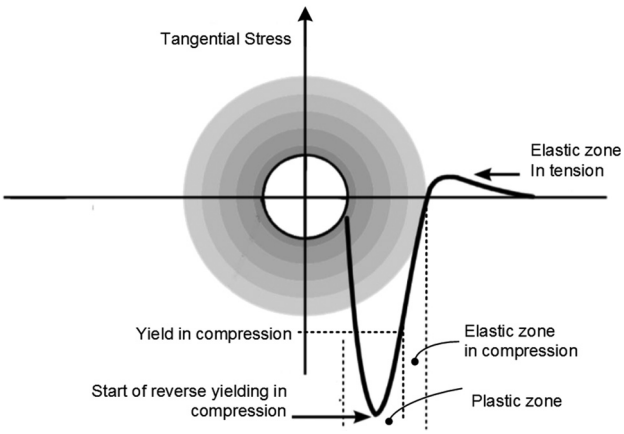

Fig. 1 Stress distribution in a cold expanded plate

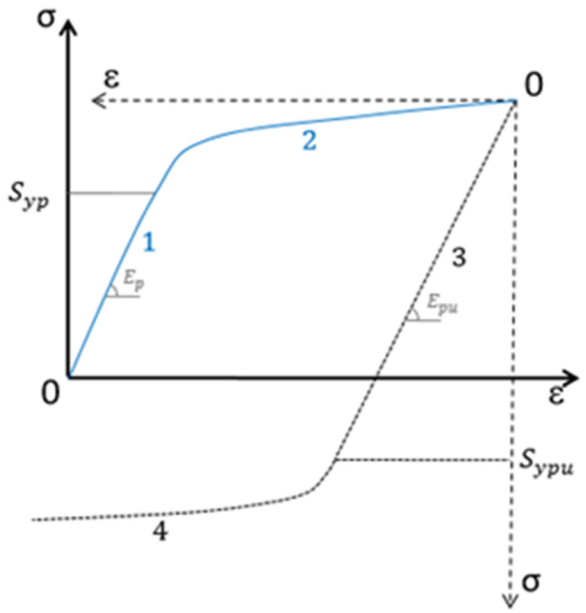

Fig. 2 Aluminum plate elasto-plastic material model

$$\varepsilon_e = \frac{\sqrt{2}}{3}\sqrt{\left[(\varepsilon_r - \varepsilon_\theta)^2 + (\varepsilon_\theta - \varepsilon_z)^2 + (\varepsilon_z - \varepsilon_r)^2\right]} \tag{5}$$

For an incompressible material in the plastic domain, the volumetric change is given by

$$\varepsilon_r + \varepsilon_\theta + \varepsilon_z = 0 \tag{6}$$

The studied model is under plane strain state, hence there is no deformation in the z direction

$$\varepsilon_z = 0 \tag{7}$$

Substituting Eq. (7) into Eq. (6) and then into Eq. (5), gives

$$\varepsilon_e = \frac{2}{\sqrt{3}}\varepsilon_\theta \tag{8}$$

According to Hencky deformation theory, the deformation in the z direction is given by

$$\varepsilon_z = \frac{3}{4}\frac{\varepsilon_e}{\sigma_e}(\sigma_z - \sigma_m) \tag{9}$$

Knowing $\varepsilon_z = 0$, gives

$$\sigma_z = \sigma_m \tag{10}$$

where σ_m the average normal stress and is given by the following relation:

$$\sigma_m = \frac{1}{3}(\sigma_r + \sigma_\theta + \sigma_z) \tag{11}$$

Therefore, the longitudinal stress in the plastic domain is given by

$$\sigma_z = \frac{1}{2}(\sigma_r + \sigma_\theta) \tag{12}$$

Substituting Eq. (12) into Eq. (4) gives

$$\sigma_e = \frac{\sqrt{3}}{2}(\sigma_\theta - \sigma_r) \tag{13}$$

Loading of the Mandrel. The mandrel being a solid shaft is subjected to an external pressure. Its radial and tangential stresses are equal to the contact pressure p_c and are both in compression, so that

$$\sigma_r = \sigma_\theta = -p_c \tag{14}$$

Considering Hooke's law under plane strain state in the axial direction

$$\varepsilon_z = \frac{1}{E_m}(\sigma_z - \nu_m(\sigma_r + \sigma_\theta)) = 0 \tag{15}$$

So

$$\sigma_z = \nu_m(\sigma_r + \sigma_\theta) \tag{16}$$

Substituting Eq. (14) into Eq. (16) gives the longitudinal stress expression in the shaft

$$\sigma_z = -2\nu_m p_c \tag{17}$$

Considering Hooke's law in the tangential direction, the expression of the tangential strain is given by

$$\varepsilon_\theta = \frac{u}{r} = \frac{1}{E_m}(\sigma_\theta - \nu_m(\sigma_z + \sigma_r)) \tag{18}$$

Substituting Eqs. (14) and (17) into Eq. (18), the radial displacement at the mandrel periphery for an elastic behavior is obtained

$$u_m = \frac{R_m p_c}{E_m}\left(2\nu_m^2 + \nu_m - 1\right) \tag{19}$$

Case 1: Plate elastic deformation

Considering the plate with a hole as a hollow cylinder of finite outside diameter subjected to internal pressure p_c, Lamé equations gives the stresses as

$$\sigma_r(r) = p_c \frac{1 - \left(\frac{R_o}{r}\right)^2}{\left(\frac{R_o}{R_i}\right)^2 - 1} \tag{20}$$

$$\sigma_\theta(r) = p_c \frac{1 + \left(\frac{R_o}{r}\right)^2}{\left(\frac{R_o}{R_i}\right)^2 - 1} \tag{21}$$

The radial displacement of a hollow cylinder subjected to internal pressure for an elastic behavior under plane strain is given by

$$u_p(r) = \frac{p_c}{E_p}\frac{(1+\nu_p)(1-2\nu_p)}{\left(\frac{R_o}{R_i}\right)^2 - 1}\left[r + \frac{1}{(1-2\nu_p)}\frac{R_o^2}{r}\right] \tag{22}$$

Considering the interference δ, the geometrical compatibility equation of displacement of the mandrel and the plate at their interface where radius $r_m = R_i$ at the end of loading, is given by:

$$\delta = u_p - u_m \tag{23}$$

This leads to the determination of the contact pressure p_c, applied at the shaft-plate hole interface in the case of an elastic behavior of the plate, such that

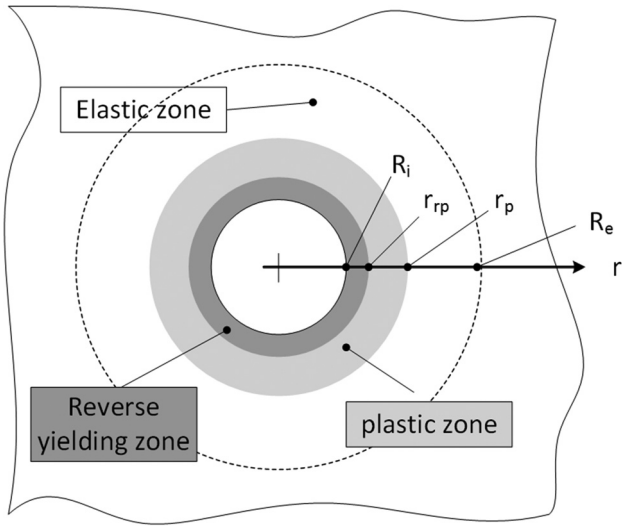

Fig. 3 Different zones near the plate hole

$$p_c = \frac{\delta}{\frac{1+\nu_p}{E_p}\left(\frac{R_o}{R_i}\right)^2 - 1}\left((1-2\nu_p)R_i + \frac{R_o^2}{R_i}\right) - \frac{R_m}{E_m}\left(2\nu_m^2 + \nu_m - 1\right) \tag{24}$$

As the interference δ increases, the plate continues to deform elastically until the contact pressure reaches a critical value equal to p_y. Starting from this point, the inner radius of the plate deforms plastically.

So, according to the von Mises criteria, the start yield occurs when

$$S_{yp} = \sigma_e \tag{25}$$

Using Eq. (13), gives

$$S_{yp} = \frac{\sqrt{3}}{2}(\sigma_\theta - \sigma_r) \tag{26}$$

According to Lamé equations, putting $p_c = p_y$

$$\sigma_\theta - \sigma_r = \frac{2p_y\left(\frac{R_o}{r}\right)^2}{\left(\frac{R_o}{R_i}\right)^2 - 1} \tag{27}$$

Therefore, the pressure p_y that causes start of yield at the plate hole radius $r = R_i$ is given by

$$p_y = \frac{S_{yp}}{\sqrt{3}}\frac{\left(\frac{R_o}{R_i}\right)^2 - 1}{\left(\frac{R_o}{R_i}\right)^2} \tag{28}$$

Case 2: Plate elasto-plastic deformation

In this case, the contact pressure exceeds the yield pressure p_y. So, the inner part of the cylinder is plastic, while the external part is still in the elastic domain. Thus, the plate exhibits an elasto-plastic behavior. The radial equilibrium equation of an infinitesimal element of a thick cylinder is given by

$$\frac{d\sigma_r}{dr} + \frac{\sigma_r - \sigma_\theta}{r} = 0 \tag{29}$$

Plastic Zone. Combining Eq. (13) and Eq. (29) and substituting for the equivalent stress in Eq. (2) in the plastic region gives

$$d\sigma_r = \frac{2}{\sqrt{3}}\left(\frac{A + B\varepsilon_e^n}{r}\right)dr \tag{30}$$

Introducing, the geometrical compatibility equations

$$\varepsilon_r = \frac{du_r}{dr} \tag{31}$$

$$\varepsilon_\theta = \frac{u_r}{r} \tag{32}$$

Substituting Eqs. (31) and (32) into Eq. (6), for a plan strain state, gives

$$\frac{du_r}{dr} = -\frac{u_r}{r} \tag{33}$$

This differential equation has a general solution of the following form:

$$u_r = \frac{D}{r} \tag{34}$$

Substituting Eqs. (34) into (32) and then using Eq. (8) gives

$$\varepsilon_e = \frac{2}{\sqrt{3}}\frac{D}{r^2} \tag{35}$$

At the elastic–plastic interface $r = r_p$, the elastic solution remains valid, and therefore

$$\varepsilon_e = \frac{S_{yp}}{E_p} \tag{36}$$

Hence, equating Eq. (35) and Eq. (36) gives the constant D, such that

$$D = \frac{S_{yp}r_p^2\sqrt{3}}{2E_p} \tag{37}$$

Substituting for D in Eq. (30) and integrating between R_i and r and noting at R_i, $\sigma_r = -p_i$ gives the expression of the radial stress in the plastic zone during loading as

$$\sigma_r(r)|_1 = -p_i + \frac{2A}{\sqrt{3}}\ln\left(\frac{r}{R_i}\right) + \frac{B}{\sqrt{3}n}\left(\frac{S_{yp}}{E_p}\right)^n\left[\left(\frac{r_p}{R_i}\right)^{2n} - \left(\frac{r_p}{r}\right)^{2n}\right] \tag{38}$$

The expression of the tangential stress σ_θ is deduced from Eqs. (29) and (38) such that

$$\sigma_\theta(r)|_1 = -p_i + \frac{2A}{\sqrt{3}}\left[\ln\left(\frac{r}{R_i}\right) + 1\right] + \frac{B}{\sqrt{3}\,n}\left(\frac{S_{yp}}{E_p}\right)^n\left[\left(\frac{r_p}{R_i}\right)^{2n} + (2n-1)\left(\frac{r_p}{r}\right)^{2n}\right] \tag{39}$$

Elastic Zone. The expressions of the radial and tangential stresses in the elastic zone of the plate ($r_p \le r \le R_o$) are given by Lamé equations as

$$\sigma_r(r)|_2 = p_{y_{r_p}}\frac{1 - \left(\frac{R_o}{r}\right)^2}{\left(\frac{R_o}{r_p}\right)^2 - 1} \tag{40}$$

$$\sigma_\theta(r)|_2 = p_{y_{r_p}}\frac{1 + \left(\frac{R_o}{r}\right)^2}{\left(\frac{R_o}{r_p}\right)^2 - 1} \tag{41}$$

Noting that $p_{y_{r_p}}$ is the pressure that causes yield to the external cylinder representing the elastic zone of the plate during loading and is given by Eq. (28). Alternatively, this pressure is equal to the radial stress at the elastic–plastic radius r_p or at the outside radius of the internal cylinder representing the elastic zone of the plate such that

$$p_{y_{r_p}} = \frac{S_{yp}}{\sqrt{3}}\frac{\left(\frac{R_o}{r_p}\right)^2 - 1}{\left(\frac{R_o}{r_p}\right)^2} = -p_i + \frac{2A}{\sqrt{3}}\ln\left(\frac{r_p}{R_i}\right) + \frac{B}{\sqrt{3}\,n}\left(\frac{S_{yp}}{E_p}\right)^n\left[\left(\frac{r_p}{R_i}\right)^{2n} - 1\right] \tag{42}$$

Furthermore, combining Eqs. (34) and (37) gives the radial displacement in the plastic zone of the plate

$$u_{r,p}(r) = \frac{\sqrt{3}\,S_{yp} r_p^2}{2E_p\, r} \tag{43}$$

In addition, using the compatibility equation given by Eq. (23) and substituting the mandrel and plate radial displacements at the contact radius u_m and u_r from Eqs. (19) and (43), respectively, gives the interface pressure p_i to cause plasticity till a radius r_p

$$p_i = \frac{E_m}{R_m\left(2\nu_m^2 + \nu_m - 1\right)}\left(\frac{\sqrt{3}}{2}\frac{S_{yp} r_p^2}{E_p R_i} - \delta\right) \tag{44}$$

Substituting for the interface pressure p_i in Eq. (42) gives the equation that can be solved to obtain the elastic–plastic radius r_p

$$\begin{aligned}\frac{S_{yp}}{\sqrt{3}}\frac{\left(\frac{R_o}{r_p}\right)^2 - 1}{\left(\frac{R_o}{r_p}\right)^2} &= \frac{E_m}{R_m\left(2\nu_m^2 + \nu_m - 1\right)}\left(\frac{\sqrt{3}}{2}\frac{S_{yp} r_p^2}{E_p R_i} - \delta\right) \\ &\quad - \frac{2A}{\sqrt{3}}\ln\left(\frac{r_p}{R_i}\right) - \frac{B}{\sqrt{3}\,n}\left(\frac{S_{yp}}{E_p}\right)^n\left[\left(\frac{r_p}{R_i}\right)^{2n} - 1\right]\end{aligned} \tag{45}$$

Step 2: Unloading of the mandrel

Once the mandrel is removed from the plate, the latter is relieved from the internal pressure. This causes a partial strain recovery. It is important to note, however, that depending on the value of the interference δ two cases can occur; a pure elastic recovery or and full elastic recovery followed by reverse plasticity.

For reverse plasticity to occur starting at the internal radius, the variation of the internal pressure should satisfy the following inequality, such that:

$$\Delta p = p_i > p_{yu} = 2p_y = \frac{S_{ypu}}{\sqrt{3}}\frac{\left(\frac{R_o}{R_i}\right)^2 - 1}{\left(\frac{R_o}{R_i}\right)^2} \tag{46}$$

In other words, the variation of the internal pressure between the loading step and the unloading step must be greater than twice the pressure p_y necessary to start yield during loading.

Case 1: Unloading without reverse yielding

The residual stresses are obtained by the superposition of the stresses applied during loading and unloading. Using Lamé equations during unloading, the stress state is

- For $R_i \le r \le r_p$

$$\sigma_r^*(r)|_1 = \sigma_r(r)|_1 - p_i\frac{1 - \left(\frac{R_o}{r}\right)^2}{\left(\frac{R_o}{r_i}\right)^2 - 1} \tag{47}$$

$$\sigma_\theta^*(r)|_1 = \sigma_\theta(r)|_1 - p_i\frac{1 + \left(\frac{R_o}{r}\right)^2}{\left(\frac{R_o}{r_i}\right)^2 - 1} \tag{48}$$

- For $r_p \le r \le R_0$

$$\sigma_r^*(r)|_2 = \sigma_r(r)|_2 - p_i\frac{1 - \left(\frac{R_o}{r}\right)^2}{\left(\frac{R_o}{r_i}\right)^2 - 1} \tag{49}$$

$$\sigma_\theta^*(r)|_2 = \sigma_\theta(r)|_2 - p_i\frac{1 + \left(\frac{R_o}{r}\right)^2}{\left(\frac{R_o}{r_i}\right)^2 - 1} \tag{50}$$

Case 2: Unloading with reverse yielding

During unloading, most of the plate will undergo an elastic recovery while part of the plate very near the bore undergoes reverse yielding. In other words, there is a new elastic–plastic radius r_{rp} that separates the two new zones during unloading. This new unloading elastic–plastic radius r_{rp} is smaller than the loading elastic–plastic radius r_p.

Similarly, the residual stresses are obtained by superposition of the stresses generated during loading and the ones during unloading. The latter are obviously dependent on the state of the initial stress and therefore the formers, such that:

- In the plastic zone

$$\begin{aligned}\sigma_r^*(r)|_1 &= \sigma_r(r)|_1 + p_i \\ &\quad - \frac{2A_u}{\sqrt{3}}\ln\left(\frac{r}{R_i}\right) - \frac{B_u}{\sqrt{3}n_u}\left(\frac{S_{ypu}}{E_{pu}}\right)^{n_u}\left[\left(\frac{r_{rp}}{R_i}\right)^{2n_u} - \left(\frac{r_{rp}}{r}\right)^{2n_u}\right]\end{aligned} \tag{51}$$

$$\begin{aligned}\sigma_\theta^*(r)|_1 &= \sigma_\theta(r)|_1 + p_i - \frac{2A_u}{\sqrt{3}}\left[\ln\left(\frac{r}{R_i}\right) + 1\right] \\ &\quad - \frac{B_u}{\sqrt{3}n_u}\left(\frac{S_{ypu}}{E_{pu}}\right)^{n_u}\left[\left(\frac{r_{rp}}{R_i}\right)^{2n_u} + (2n_u - 1)\left(\frac{r_{rp}}{r}\right)^{2n_u}\right]\end{aligned} \tag{52}$$

- In the elastic zone
- For $r_{rp} \le r \le r_p$

$$\sigma_r^*(r)|_2 = \sigma_r(r)|_1 - p_{yu_{rrp}}\frac{1 - \left(\frac{R_o}{r}\right)^2}{\left(\frac{R_o}{r_{rp}}\right)^2 - 1} \tag{53}$$

$$\sigma_\theta^*(r)|_2 = \sigma_\theta(r)|_1 - p_{yu_{rrp}}\frac{1 + \left(\frac{R_o}{r}\right)^2}{\left(\frac{R_o}{r_{rp}}\right)^2 - 1} \tag{54}$$

- For $r_p \le r \le R_o$

$$\sigma_r^*(r)|_3 = \sigma_r(r)|_2 - p_{yu_{rrp}}\frac{1 - \left(\frac{R_o}{r}\right)^2}{\left(\frac{R_o}{r_{rp}}\right)^2 - 1} \tag{55}$$

$$\sigma_\theta^*(r)|_3 = \sigma_\theta(r)|_2 - p_{yu_{rrp}}\frac{1 + \left(\frac{R_o}{r}\right)^2}{\left(\frac{R_o}{r_{rp}}\right)^2 - 1} \tag{56}$$

The unloading elastic–plastic radius r_{rp} is determined by the same approach as the one used to find the loading elastic–plastic radius r_p of the plastic zone. That is to say that during unloading, the radial stress of the inner cylinder at the new interface is equal to the pressure required to yield the outer cylinder. So, for $r = r_{rp}$ we have:

$$\begin{cases} \sigma_r(r_{rp})|_u = -p_{yu_{r_{rp}}} \\ p_{yu_{r_{rp}}} = \dfrac{S_{\text{ypu}}}{\sqrt{3}} \dfrac{\left(\dfrac{R_o}{r_{rp}}\right)^2 - 1}{\left(\dfrac{R_o}{r_{rp}}\right)^2} \end{cases} \tag{57}$$

where $\sigma_r(r)|_u$ it is the radial stress during unloading and is given by

$$\sigma_r(r)|_u = -p_i + \frac{2A_u}{\sqrt{3}} \ln\left(\frac{r}{R_i}\right) + \frac{B_u}{\sqrt{3}n_u} \left(\frac{S_{\text{ypu}}}{E_{pu}}\right)^{n_u} \left[\left(\frac{r_{rp}}{R_i}\right)^{2n_u} - \left(\frac{r_{rp}}{r}\right)^{2n_u}\right] \tag{58}$$

This radial stress is obtained by the same reasoning applied to obtain the radial stress of the plastic zone of Eq. (38) during loading. Therefore, the radius r_{rp} is obtained by the solving the following expression:

$$\frac{S_{\text{ypu}}}{\sqrt{3}} \frac{\left(\frac{R_o}{r_{rp}}\right)^2 - 1}{\left(\frac{R_o}{r_{rp}}\right)^2} = p_i - \frac{2A_u}{\sqrt{3}} \ln\left(\frac{r_{rp}}{R_i}\right) - \frac{B_u}{\sqrt{3}n_u} \left(\frac{S_{\text{ypu}}}{E_{pu}}\right)^{n_u} \left[\left(\frac{r_{rp}}{R_i}\right)^{2n_u} - 1\right] \tag{59}$$

The radial, longitudinal, hoop, and equivalent residual stress are therefore identified for every zone during loading and unloading and with and without reverse yielding and are given in the Appendix. A MATLAB code was written to obtain the residual stresses for the treated cases.

Numerical Finite Element Method Validation

In this part, ANSYS Workbench platform was used to model the expansion process of a hole of an aluminum alloy plate subjected to the cold strain hardening. The materials and geometry adopted to illustrate the cold expansion process are shown in Table 1. Using the symmetry in the y direction, the model is defined by two-dimensional axisymmetric isoparametric eight-node elements. The mesh shown in Fig. 4 was made directly on the platform under the static structure option of the ANSYS software. To do this, the geometrical model was discretized using a sufficiently refined mesh in order to obtain accurate stresses at the area of contact between the mandrel and the plate. A mesh convergence criterion of 1% on the equivalent stress at the bore was adopted. In order to model the material elasto-plastic behavior, the multilinear kinematic hardening function was used, while for the case of the mandrel material, only the elastic behavior has been considered by introducing the Young modulus and the Poisson's ratio of the steel material. Target and contact elements without friction were used to model the interface between the mandrel and the aluminum plate at the bore.

Table 1 Geometry and material properties

	Mandrel AISI 4340	Plate Al-7050-T73511
R_o (mm)	—	$10R_i$
r_m, R_i (mm)	$R_i + \delta$	2.5
S_{ym}, S_{yp} (MPa)	710	434
S_{ypu} (MPa)	—	$2S_{yp}$
ν_m, ν_p	0.29	0.33
ν_{pu}	—	0.33
E_m, E_p (GPa)	205	71.7
E_{pu} (GPa)	—	71.7
A (MPa)	—	5.05
A_u (MPa)	—	8.28
B (MPa)	—	550
B_u (MPa)	—	931
n	—	0.06534
n_u	—	0.03906
δ (mm)	0.01 to 0.1	

During the simulation, the following boundary conditions are applied to the plate and the mandrel; the node that belong to the plate lower surface were blocked in the normal direction, and the flat end of the mandrel was allowed to move by imposing a displacement in the direction of its axis. The constraint of the plate in the y direction was to simplify the analysis by avoiding bending and compare the residual stresses due expansion only. In practice, even though the plate is supported at some distance from the bore, the bending effect is expected to be small. The loading and unloading steps are produce by the complete displacement of the mandrel. The analytical stresses are compared to those located at the midthickness of the plate.

Results and Discussion

In order to study aluminum sheets subjected to cold expansion with a mandrel and illustrate the effect of reverse yielding on the residual stresses near the bore, a case study was considered with an aluminum an alloy plate having a hole with a radius of 2.5 mm and different interferences. It is worth noting again that the plate is modeled as a cylinder having a ratio of inner and outer radii equals to 10 in order to get closer to the rectangular plate behavior case as much as possible.

The study involves obviously varying the interference to investigate its effect on the residual stresses. A total of five different interference values from 0.01 to 0.1 mm were considered. The calculations show that the magnitude of the stresses depends strongly on the value of the interference, and that the stresses increase with the increase of the value of the interference. The distribution of all stresses shows a decrease with the radial position until the stresses becomes zero and particularly during unloading. Figures 5–8 show the radial, longitudinal, hoop, and equivalent stresses, respectively, during loading and Figs. 9–12 show the residual stresses during unloading with reverse yielding taking place.

In general, the stresses obtained from the analytical model are in good agreement with those of FEM for all ranges of interference. Nevertheless, the highest difference is with the highest interference of 0.08 mm where the predicted stresses at the elasto-plastic radii of both the loading and unloading phases are higher than those of FEM. This is believed to be caused by the tolerance

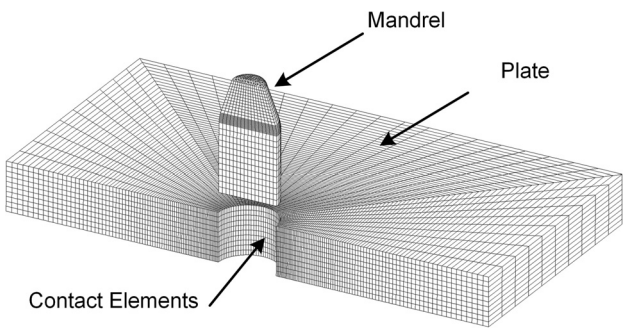

Fig. 4 Axisymmetric FE model

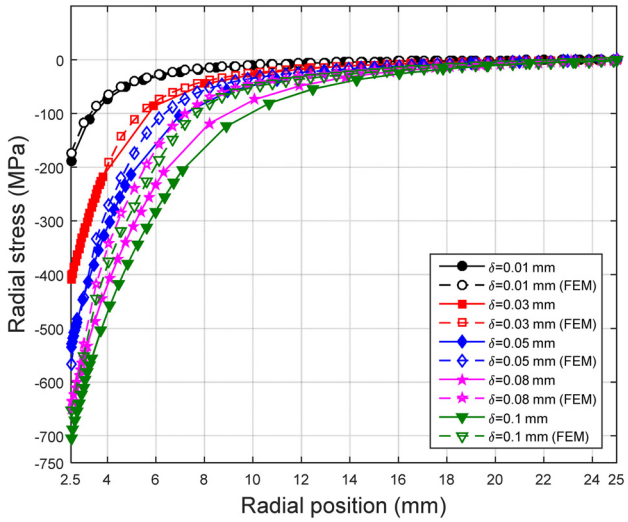

Fig. 5 Radial stresses—during loading

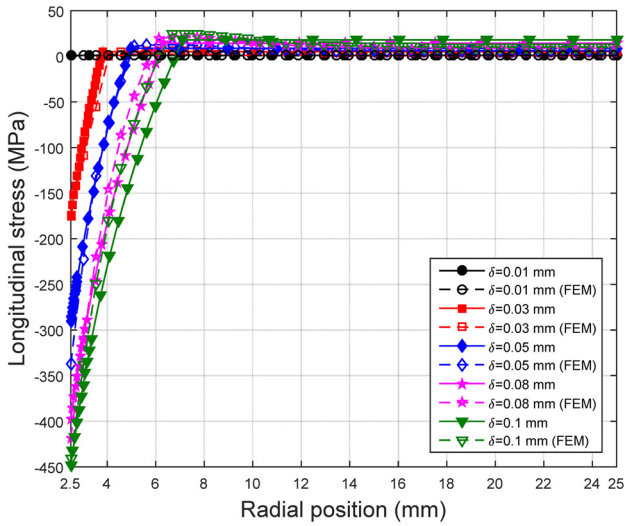

Fig. 6 Longitudinal stresses—during loading

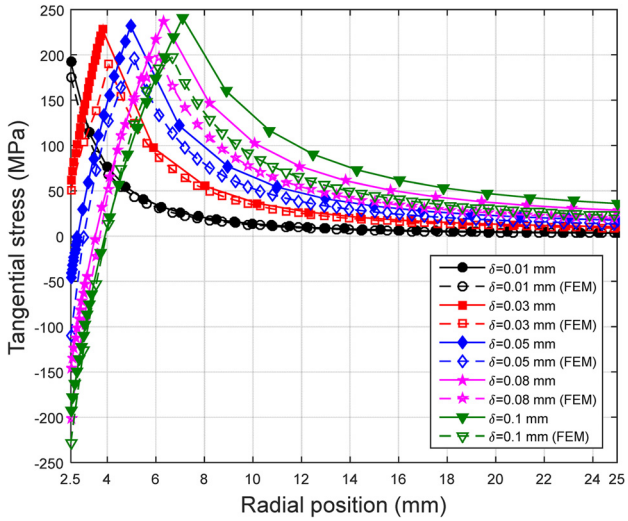

Fig. 7 Hoop stresses—during loading

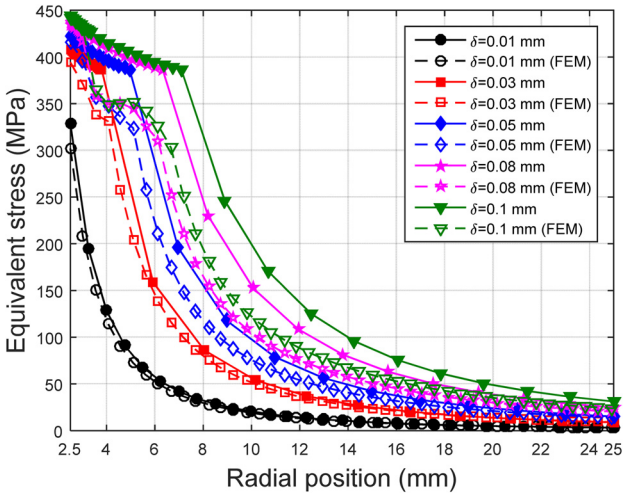

Fig. 8 Equivalent stresses—during loading

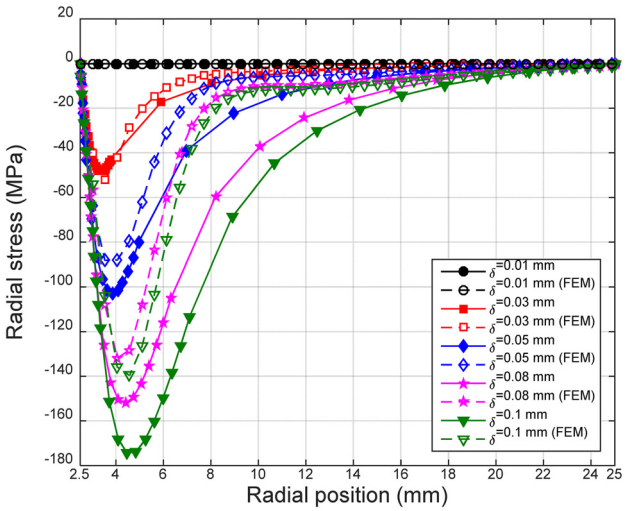

Fig. 9 Residual radial stresses—effect of reverse yielding

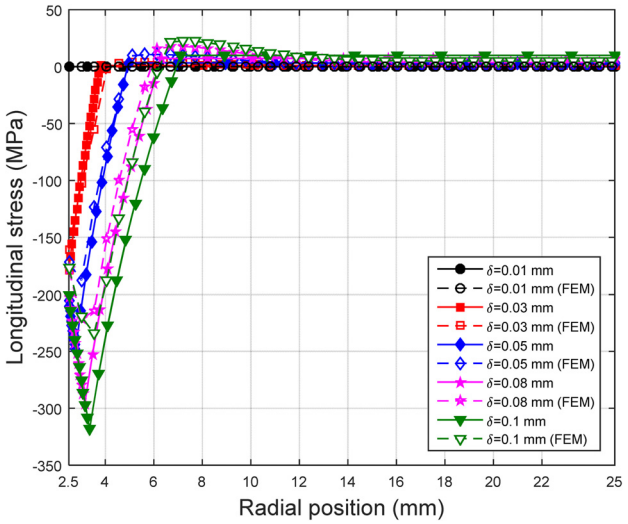

Fig. 10 Residual longitudinal stresses—effect of reverse yielding

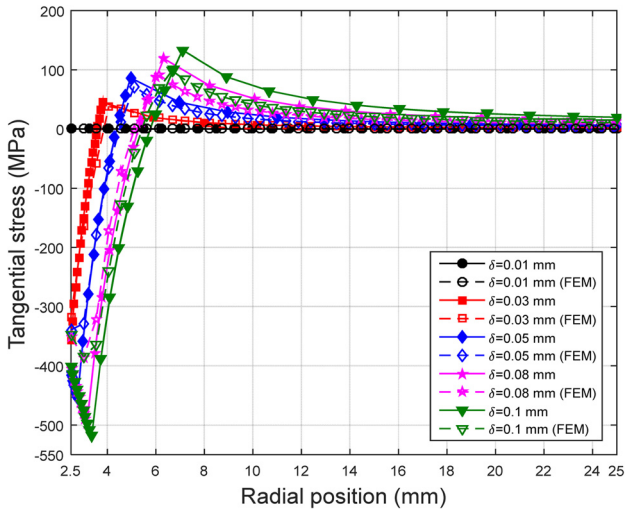

Fig. 11 Residual hoop stresses—effect of reverse yielding

option in the actual contact position or penetration with ANSYS that requires adjustment. Otherwise, the general trend is the same in both cases. It is clear that above 0.01 mm of interference, the aluminum plate starts to deform plastically. The radial stress at 2.5 mm gives the contact pressure below which there are no residual stresses as shown in Figs. 8 and 12 where the equivalent stress is null. Above this value of interference, plastic deformation starts at the inside radius and works its way through the plate.

In addition, it should be noted that when the interference values are large, the plate is in elasto-plastic behavior in both loading and unloading confirming reverse yielding. It is also noted that for larger interference values, the residual stresses exceed the value of the ultimate stress, which may possibly cause necking and damage to the assembly in addition of being the limiting case for the validity of the model. The hoop and longitudinal stress distributions show a sudden reverse of the curves that occurs at one or two millimeters from the bore indicating the presence of reverse yielding. This is well indicated by both the analytical and FE results. The none consideration of Bauschinger effect will overestimate the residual stresses and is not representative of the real behavior. The residual equivalent stress of this small region is shown in Fig. 12 to be around the yield stress.

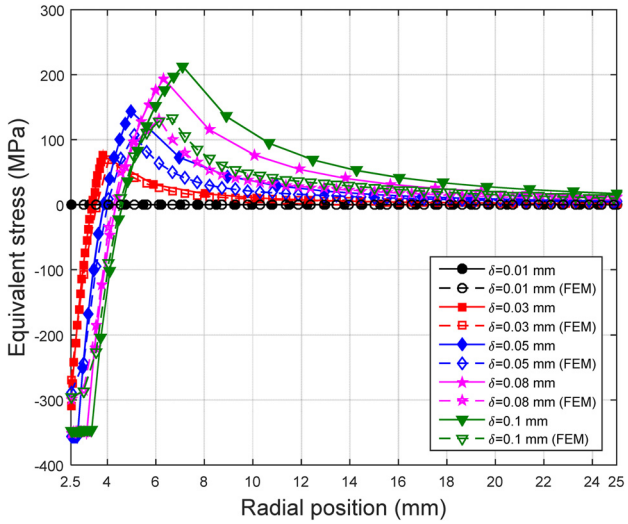

Fig. 12 Residual equivalent stresses—effect of reverse yielding

If, however, the values of the interference are low, it is found that the plate has an elasto-plastic behavior during loading and a purely elastic behavior during unloading. Indeed, this occurs for an interference value smaller than 0.03 mm. This support the assertion that the behavior of the plate strongly depends on the value of the interference. As a result, in the case where the plate is plastically deformed and the case where a reverse yielding of the plate occurs, a set of formulae of stresses during loading and residual stresses during unloading is grouped into the special form in the Appendix for ease of use by the interested reader.

Conclusion

An analytical model that predicts the residual stresses in an aluminum plate subjected to cold expansion was developed and a set of formulae to predict the residual stress were successfully implemented in a MATLAB code. In general, it was found that the stress distributions obtained with the analytical model are in good agreement with those generated by FE modelling for both the loading and unloading phases. However, a slight difference between the two methods was observed at high interference particularly during unloading where the difference is somehow more pronounced. Indeed, the graphs show that the higher the interference value, the greater the difference between the two methods is obtained. This is attributed to the fact that the FE contact tolerance option should be tighter.

It is clear that the model predicts reverse yielding adequately. The hoop and longitudinal stresses show a sharp reverse in the curves near the bore due to reverse yielding without which the stresses are overestimated. This model is a very useful tool to verify the interference required to obtain desired residual stresses in a cold expanded aluminum plate.

Nomenclature

A, B = loading plasticity constants (MPa)
A_u, B_u = unloading plasticity constants (MPa)
D = integration constant
E_m = elastic modulus of the mandrel (MPa)
E_p, E_{pu} = plate loading and unloading elastic modulus (MPa)
n, n_u = plate loading and unloading strain hardening exponents
p_i = inner pressure (MPa)
p_y, p_{yu} = contact pressure to start yield during loading and unloading (MPa)
$p_{y_{rp}}, p_{yu_{rp}}$ = pressure that causes yield to the elastic zone of the plate loading and unloading
r = radius (mm)
r_p, r_{rp} = loading and unloading elastic-plastic radius (mm)
R_m = mandrel radius (mm)
R_i, R_o = inner and outer plate radii (mm)
S_{yp}, S_{ypu} = plate loading and unloading yield stress (MPa)
u_r = radial displacement (mm)
$u_{r,m}$, $u_{r,p}$ = radial displacement of mandrel and plate (mm)
δ = interference (mm)
ε_e = equivalent strain (mm/mm)
$\varepsilon_r, \varepsilon_\theta, \varepsilon_z$ = radial, hoop, and longitudinal strains (mm/mm)
ν_m, ν_p = Poisson's ratio of mandrel and plate
ν_{pu} = Poisson's ratio of plate during unloading
σ_e = equivalent stress (MPa)
$\sigma_e|_l$ = equivalent stress loading (MPa)
$\sigma_r, \sigma_\theta, \sigma_z$ = radial, hoop, and longitudinal stresses (MPa)
$\sigma_r|_u$ = radial stress during unloading (MPa)
$\sigma_r|_l$ = radial stress loading (MPa)
$\sigma_z|_l$ = longitudinal stress loading (MPa)
$\sigma_\theta|_l$ = hoop stress loading (MPa)
$\sigma_r^*, \sigma_\theta^*, \sigma_z^*, \sigma_e^*$ = residual stresses (MPa)

Appendix

For the case where a reverse yielding of the plate occurs, a set of formulae for stresses during loading and unloading is grouped in this appendix for ease and clarity to the reader:

- Stresses during loading

$$R_i \le r \le r_p$$

$$\begin{cases} \sigma_r(r)|_1 = -p_i + \dfrac{2A}{\sqrt{3}}\ln\left(\dfrac{r}{R_i}\right) + \dfrac{B}{\sqrt{3}\,n}\left(\dfrac{S_{yp}}{E_p}\right)^n \\ \qquad \times\left[\left(\dfrac{r_p}{R_i}\right)^{2n} - \left(\dfrac{r_p}{r}\right)^{2n}\right] \\ \sigma_\theta(r)|_1 = -p_i + \dfrac{2A}{\sqrt{3}}\left[\ln\left(\dfrac{r}{R_i}\right) + 1\right] + \dfrac{B}{\sqrt{3}\,n}\left(\dfrac{S_{yp}}{E_p}\right)^n \\ \qquad \times\left[\left(\dfrac{r_p}{R_i}\right)^{2n} + (2n-1)\left(\dfrac{r_p}{r}\right)^{2n}\right] \\ \sigma_z(r)|_1 = \dfrac{1}{2}(\sigma_r(r)|_1 + \sigma_\theta(r)|_1) \\ |_1 = \dfrac{\sqrt{3}}{2}(\sigma_\theta(r)|_1 - \sigma_r(r)|_1) \end{cases} \tag{A1}$$

$$r_p \le r \le R_o$$

$$\begin{cases} \sigma_r(r)|_2 = p_{y_{rp}}\dfrac{1-\left(\dfrac{R_o}{r}\right)^2}{\left(\dfrac{R_o}{r_p}\right)^2 - 1} \\ \sigma_\theta(r)|_2 = p_{y_{rp}}\dfrac{1+\left(\dfrac{R_o}{r}\right)^2}{\left(\dfrac{R_o}{r_p}\right)^2 - 1} \\ \sigma_z(r)|_2 = \nu_p(\sigma_r(r)|_2 + \sigma_\theta(r)|_2) \\ \sigma_e(r)|_2 = \dfrac{\sqrt{3}}{2}(\sigma_\theta(r)|_2 - \sigma_r(r)|_2) \end{cases} \tag{A2}$$

- Residual stresses after unloading

$$R_i \le r \le r_{rp}$$

$$\begin{cases} \sigma_r^*(r)|_1 = \sigma_r(r)|_1 + p_i - \dfrac{2A_u}{\sqrt{3}}\ln\left(\dfrac{r}{R_i}\right) \\ -\dfrac{B_u}{\sqrt{3}n_u}\left(\dfrac{S_{\text{ypu}}}{E_{pu}}\right)^{n_u}\left[\left(\dfrac{r_{rp}}{R_i}\right)^{2n_u} - \left(\dfrac{r_{rp}}{r}\right)^{2n_u}\right] \\ \sigma_\theta^*(r)|_1 = \sigma_\theta(r)|_1 + p_i - \dfrac{2A_u}{\sqrt{3}}\left[\ln\left(\dfrac{r}{R_i}\right) + 1\right] \\ -\dfrac{B_u}{\sqrt{3}n_u}\left(\dfrac{S_{\text{ypu}}}{E_{pu}}\right)^{n_u}\left[\left(\dfrac{r_{rp}}{R_i}\right)^{2n_u} + (2n-1)\left(\dfrac{r_{rp}}{r}\right)^{2n_u}\right] \\ \sigma_z^*(r)|_1 = \dfrac{1}{2}(\sigma_r^*(r)|_1 + \sigma_\theta^*(r)|_1) \\ \sigma_e^*(r)|_1 = \dfrac{\sqrt{3}}{2}(\sigma_\theta^*(r)|_1 - \sigma_r^*(r)|_1) \end{cases} \tag{A3}$$

$$r_{rp} \le r \le r_p$$

$$\begin{cases} \sigma_r^*(r)|_2 = \sigma_r(r)|_1 - p_{yu_{rrp}}\dfrac{1-\left(\dfrac{R_o}{r}\right)^2}{\left(\dfrac{R_o}{r_{rp}}\right)^2 - 1} \\ \sigma_\theta^*(r)|_2 = \sigma_\theta(r)|_1 - p_{yu_{rrp}}\dfrac{1+\left(\dfrac{R_o}{r}\right)^2}{\left(\dfrac{R_o}{r_{rp}}\right)^2 - 1} \\ \sigma_z^*(r)|_2 = \nu_{up}(\sigma_r^*(r)|_2 + \sigma_\theta^*(r)|_2) \\ \sigma_e^*(r)|_2 = \dfrac{\sqrt{3}}{2}(\sigma_\theta^*(r)|_2 - \sigma_r^*(r)_2|) \end{cases} \tag{A4}$$

$$r_p \le r \le R_o$$

$$\begin{cases} \sigma_r^*(r)|_3 = \sigma_r(r)|_2 - p_{yu_{rrp}}\dfrac{1-\left(\dfrac{R_o}{r}\right)^2}{\left(\dfrac{R_o}{r_{rp}}\right)^2 - 1}| \\ \sigma_\theta^*(r)|_3 = \sigma_\theta(r)|_2 - p_{yu_{rrp}}\dfrac{1+\left(\dfrac{R_o}{r}\right)^2}{\left(\dfrac{R_o}{r_{rp}}\right)^2 - 1} \\ \sigma_z^*(r)|_3 = \nu_{up}(\sigma_r^*(r)|_3 + \sigma_\theta^*(r)|_3) \\ \sigma_e^*(r)|_3 = \dfrac{\sqrt{3}}{2}(\sigma_\theta^*(r)|_3 - \sigma_r^*(r)|_3) \end{cases} \tag{A5}$$

References

[1] Fu, Y., Ge, E., Su, H., Xu, J., and Li, R., 2015, "Cold Expansion Technology of Connection Holes in Aircraft Structures: A Review and Prospect," Chin. J. Aeronaut., **28**(4), pp. 961–973.

[2] Taylor, G. I., 1948, "The Formation and Enlargement of a Circular Hole in a Thin Plastic Sheet," Q. J. Mech. Appl. Math., **1**(1), pp. 103–124.

[3] Mangasarian, O. L., 1960, "Stress in the Plastic Range Around a Normally Loaded Circular Role in an Infinite Sheet," ASME J. Appl. Mech., **27**(1), pp. 65–73.

[4] Frocht, M. M., and Hill, H., 1940, "Stress-Concentration Factors Around a Central Circular Hole in a Plate Loaded Through a Pin in the Hole," J. Appl. Mech., v. 7, pp. A5–A10.

[5] Phillips, J. L., 1974, "*Sleeve Cold Working Fastener Holes*," Vol. 1, Air Force Materials Laboratory, Wright-Patterson AFB, OH, Report No. AFML-TR-74-10.

[6] Liu, J., Xu, H. L., Zhai, H. B., and Yue, Z. F., 2010, "Effect of Detail Design on Fatigue Performance of Fastener Hole," Mater. Des., **31**(2), pp. 976–980.

[7] Liu, J., Yue, Z. F., and Liu, Y. S., 2007, "Surface Finish of Open Holes on Fatigue Life," Theor. Appl. Fract. Mech., **47**(1), pp. 35–45.

[8] Garcia-Granada, A., Lacarac, V., Smith, D., Pavier, M., Cook, R., and Holdway, P., 1999, "3D Residual Stresses Around Cold Expanded Holes in a New Creep Resistant Aluminium Alloy," WIT Trans. Eng. Sci., **25**, pp. 103–116.

[9] Cook, R., and Holdway, P., 1993, "Residual Stresses Induced by Hole Cold Expansion," WIT Trans. Eng. Sci., **2**, pp. 91–100.

[10] Zhang, Y., Fitzpatrick, M., and Edwards, L., 2005, "Analysis of the Residual Stress Around a Cold-Expanded Fastener Hole in a Finite Plate," Strain, **41**(2), pp. 59–70.

[11] De Matos, P., Moreira, P., Camanho, P., and De Castro, P., 2005, "Numerical Simulation of Cold Working of Rivet Holes," Finite Elem. Anal. Des., **414** (9–10), pp. 989–1007.

[12] Clark, G., 1991, "Modelling Residual Stresses and Fatigue Crack Growth at Cold Expanded Fastener Holes," Fatigue Fract. Eng. Mater. Struct., **14**(5), pp. 579–589.

[13] Nadai, A., 1943, "Theory of Expanding of Boiler and Condenser Tube Joints Through Rolling," Trans. ASME, **65**(8), pp. 865–877.

[14] Rich, D. L., and Impellizzeri, L. F., 1977, "Fatigue Analysis of Cold-Worked and Interference Fit Fastener Holes," *Cyclic Stress–Strain and Plastic Deformation Aspects of Fatigue Crack Growth*, American Society for Testing and Materials, Philadelphia, PA, No. ASTM STP 637, pp. 153–175.

[15] Hsu, Y., and Forman, R., 1975, "Elastic-Plastic Analysis of an Infinite Sheet Having a Circular Hole Under Pressure," ASME J. Appl. Mech., **42**(2), pp. 347–352.

[16] Guo, W., 1993, "Elastic–Plastic Analysis of a Finite Sheet With a Cold-Worked Hole," Eng. Fract. Mech., **45**, pp. 857–864.
[17] Wang, G. S., 1988, "An Elastic-Plastic Solution for a Normally Loaded Center Hole in a Finite Circular Body," Int. J. Pressure Vessel Piping, **33**(4), pp. 269–284.
[18] Poussard, C., Pavier, M., and Smith, D., 1995, "Analytical and Finite Element Predictions of Residual Stresses in Cold Worked Fastener Holes," J. Strain Anal. Eng. Des., **30**(4), pp. 291–304.
[19] Ball, D., 1995, "Elastic-Plastic Stress Analysis of Cold Expanded Fastener Holes," Fatigue Fract. Eng. Mater. Struct., **18**(1), pp. 47–63.
[20] Lapalme, M., 2013, "Caractérisation des Contraintes Résiduelles Engendrées par l'Expansion à Froid de Trous dans des Alliages d'Aluminium," Master thesis, École Polytechnique de Montréal, Montreal, QC, Canada.
[21] Dietrich, G., and Potter, J. M., 1976, "Stress Measurements on Cold-Worked Fastener Holes," Adv. X-Ray Anal., **20**, pp. 321–328.
[22] Poolsuk, S., and Sharpe, W. N., Jr., 1978, "Measurement of the Elastic–Plastic Boundary Around Coldworked Fastener Holes," Trans. ASME J. Appl. Mech., **45**(3), pp. 515–520.
[23] Petersen, D. R., Arora, P. R., Dattaguru, B., and Subramańya Hande, H. S., 1992, "A Method for Estimation of the Radius of Elastic–Plastic Boundary Around Cold-Worked Holes," J. Test. Eval., **20**(5), pp. 369–375.
[24] Laghzale, N., and Bouzid, A., 2016, "Analytical Modelling of Elastic-Plastic Interference Fit Joints," Int. Rev. Modell. Simul., **9**(3), pp. 191–199.
[25] Bouzid, A., and Kazeminia, M., 2016, "Effect of Reverse Yielding on the Residual Contact Pressure in Tube-to-Tubesheet Joints," ASME J. Pressure Vessel Technol., **138**(6), p. 061406.
[26] Ludwik, P., 1909, *Element Der Technologischen Mechanik*, Springer, Berlin, pp. 32–44.